BIOCHEMISTRY
including biophysical chemistry & molecular biology

Article

pubs.acs.org/biochemistry

Analysis of SecA Dimerization in Solution

Andy J. Wowor,[†] Yuetian Yan,[‡] Sarah M. Auclair,[†] Dongmei Yu,[†] Jun Zhang,[‡] Eric R. May,[§] Michael L. Gross,[‡] Debra A. Kendall,[†] and James L. Cole*[,§,∥]

[†]Department of Pharmaceutical Sciences, University of Connecticut, Storrs, Connecticut 06269, United States

[‡]Department of Chemistry, Washington University, St. Louis, Missouri 63130, United States

[§]Department of Molecular and Cell Biology, University of Connecticut, Storrs, Connecticut 06269, United States

[∥]Department of Chemistry, University of Connecticut, Storrs, Connecticut 06269, United States

Supporting Information

ABSTRACT: The Sec pathway mediates translocation of protein across the inner membrane of bacteria. SecA is a motor protein that drives translocation of preprotein through the SecYEG channel. SecA reversibly dimerizes under physiological conditions, but different dimer interfaces have been observed in SecA crystal structures. Here, we have used biophysical approaches to address the nature of the SecA dimer that exists in solution. We have taken advantage of the extreme salt sensitivity of SecA dimerization to compare the rates of hydrogen−deuterium exchange of the monomer and dimer and have analyzed the effects of single-alanine substitutions on dimerization affinity. Our results support the antiparallel dimer arrangement observed in one of the crystal structures of *Bacillus subtilis* SecA. Additional residues lying within the preprotein binding domain and the C-terminus are also protected from exchange upon dimerization, indicating linkage to a conformational transition of the preprotein binding domain from an open to a closed state. In agreement with this interpretation, normal mode analysis demonstrates that the SecA dimer interface influences the global dynamics of SecA such that dimerization stabilizes the closed conformation.

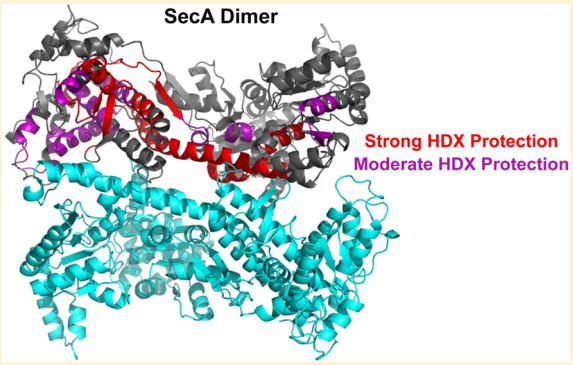

In bacteria, a majority of secretory preproteins are translocated through a general secretion (Sec) pathway that contains a Sec translocase complex comprising the integral membrane channel, SecYEG, and the cytosolic ATPase motor protein, SecA.[1,2] SecA binds preproteins, associates with the SecYEG channel, and harnesses energy from ATP hydrolysis to drive conformational changes that lead to preprotein translocation.[3−6] SecA is a large, 102 kDa multifunctional protein that is composed of several domains: nucleotide binding domains I and II (NBD I and II, respectively), a preprotein binding domain (PBD), and a C-domain that is composed of an α-helical scaffold domain (HSD), an α-helical wing domain (HWD), and a carboxyl-terminal linker (CTL) (Figure 1).[7] The PBD and HWD contribute to the formation of a binding groove for the signal peptide region of the preprotein.[8−12]

SecA exists in a monomer−dimer equilibrium that is sensitive to salt concentration and temperature.[13−16] The cellular concentration of SecA is 5−8 μM,[17,18] and its dissociation constant is 0.28 μM in 200 mM KCl.[16] Thus, in the absence of ligands, SecA likely exists as a dimer in the cytoplasm.[13,16] It has been suggested that SecA functions as a dimer during preprotein translocation because a cross-linked SecA dimer[19,20] and a genetically produced SecA dimer[21] are active for translocation. Nevertheless, the oligomeric state of SecA during preprotein translocation remains controversial. Some studies indicate that dissociation of SecA is favored in the presence of phospholipids[18,22] or synthetic signal peptides,[23] and upon SecYEG binding.[24] Other reports support an active monomeric form of SecA, indicating that the monomeric SecA mutant is functional,[25] whereas a disulfide cross-linked dimer is nonfunctional and its reduced monomeric counterpart functional.[26]

The relative positioning of the two protomers in the SecA dimer is also unclear. Although the structure of the SecA protomer obtained from different bacterial species is highly conserved in crystal structures, multiple dimeric interfaces have been identified[27−31] among the five crystal structures of the SecA dimer reported to date (Figure 2). Both parallel[29] and antiparallel[27,28,30,31] dimer orientations are observed, and these structures contain different dimerization interfaces. For example, the dimer interface of *Escherichia coli* SecA (PDB entry 2FSF)[31] lies on the opposite side relative to the dimer interface in one of the *Bacillus subtilis* SecA structures (PDB entry 1M6N).[27] It is difficult to distinguish crystal packing contacts from biologically relevant protein−protein interfaces,[7,32,33] and it remains unclear which of these crystal

Received: March 21, 2014
Revised: April 30, 2014
Published: May 1, 2014

   dx.doi.org/10.1021/bi500348p | *Biochemistry* 2014, 53, 3248−3260

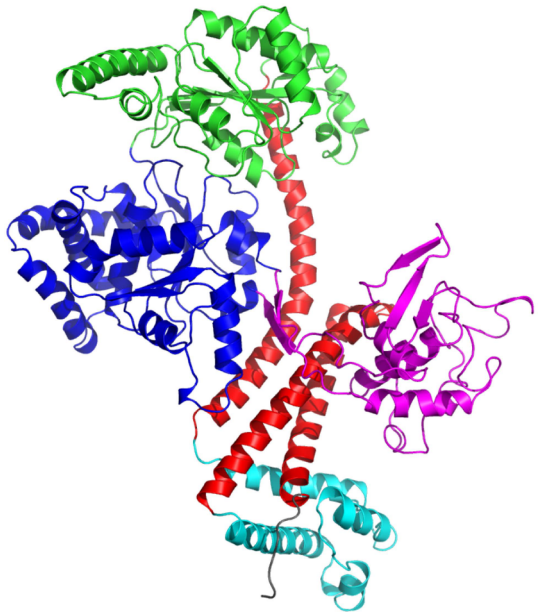

Figure 1. Structural domains of SecA. The structure of *Escherichia coli* SecA (PDB entry 2VDA)[8] with domains indicated by color: blue for NBD I, purple for PBD, green for NBD II, red for HSD, and cyan for HWD. In this monomer structure, the PBD adopts an open conformation.

structures, if any, corresponds to the physiologically relevant SecA dimer. Single-particle cryo-electron microscopy measurements support an antiparallel dimer structure,[14] and fluorescence resonance energy transfer distance measurements show the greatest agreement with the 1M6N antiparallel dimer.[34,35] A cross-linking study led to the proposal of a novel interface that involves residues from NBD I, the PBD, and the HSD.[36]

Interestingly, the PBD is found to adopt multiple conformations. A closed form that brings the PBD and HWD into the proximity of each other is found in several SecA dimer crystal structures[27−29] and in a structure of a SecA monomer complexed with ADP,[37] whereas an open conformation in which the PBD is solvent accessible exists in a crystal structure of a monomeric form[38] and in one dimer structure.[31] In the open state, the groove between the PBD and NBD II forms a polypeptide-binding clamp.[24,39] Binding of a non-signal sequence peptide in this region results in movement of the PBD toward NBD II.[37] Interaction of SecA with SecYEG induces further movement of the PBD toward NBD II, closing the clamp.[24] Nuclear magnetic resonance (NMR) analysis indicates that SecA interconverts between open and closed states in solution, with the equilibrium favoring the open state.[8] Cysteine cross-linking indicates that movement of the PBD from the open state to the closed clamp state is required for the initiation of translocation.[40]

To resolve these conflicting interpretations, we report here the use of three biophysical strategies to identify the dimer interface of SecA in solution and to characterize the conformational changes associated with dimerization. First, we used hydrogen−deuterium exchange mass spectrometry (HDX MS) to identify regions on SecA that are protected from exchange upon dimerization and to probe conformational changes associated with dimerization. To allow studies of the monomer and dimer at comparable concentrations, we took advantage of the extreme salt dependence for dimerization of SecA to preferentially form either the SecA monomer or the dimer. Second, to complement the result from HDX and gain site-specific information about the dimer interface, we selected amino acids for alanine substitution that are predicted to make significant energetic contributions to SecA dimerization based on alternative dimer interfaces. Each alanine-substituted protein was then analyzed by sedimentation velocity analytical ultracentrifugation (AUC) to measure SecA dimerization

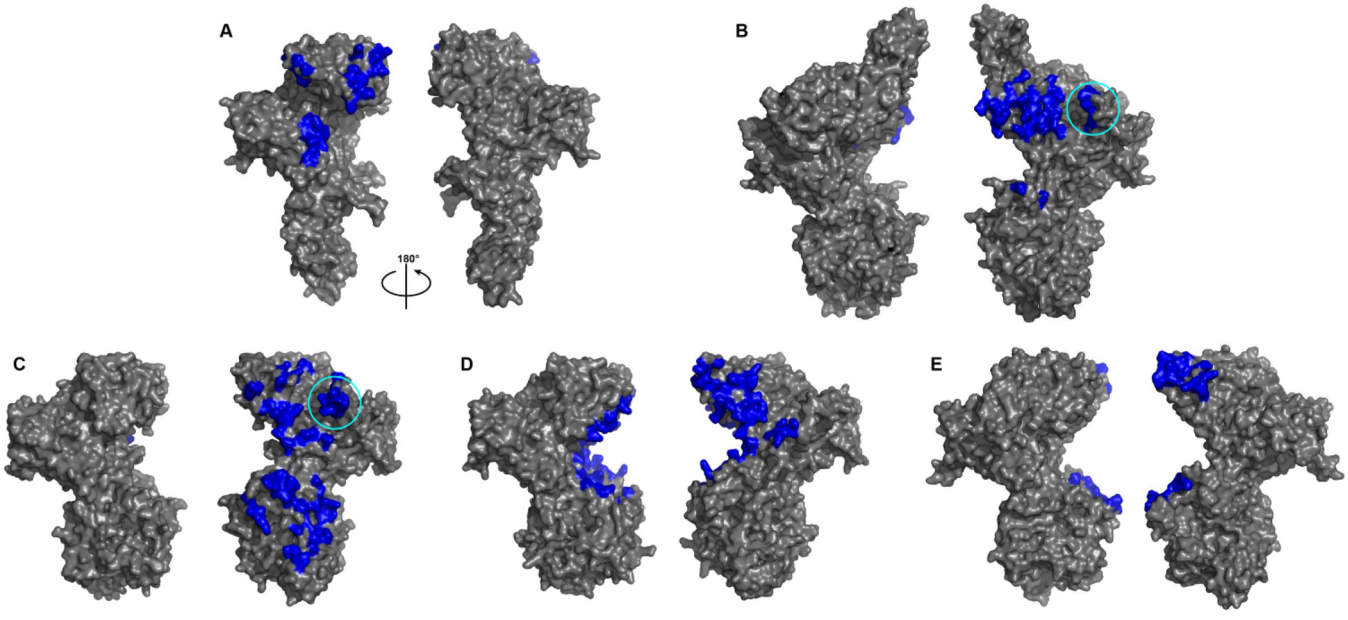

Figure 2. Alternative dimer interfaces in SecA. The dimer interfaces in different structures of SecA are colored blue with the protomers in two orientations. (A) *E. coli* SecA (PDB entry 2FSF),[31] (B) *Thermus thermophilus* (PDB entry 2IPC),[29] (C) *B. subtilis* (PDB entry 1M6N),[27] (D) *B. subtilis* (PDB entry 2IBM),[30] and (E) *Mycobacterium tuberculosis* (PDB entry 1NL3).[28] The cyan circles in panels B and C indicate the location of the N-terminal region.

dx.doi.org/10.1021/bi500348p | *Biochemistry* 2014, 53, 3248−3260

affinity. Third, we conducted normal mode analysis of the SecA monomer and dimer and defined conformational changes linked to dimerization. This combined strategy locates the likely SecA dimer interface and provides a link between closure of the PBD−HWD groove and SecA dimerization.

MATERIALS AND METHODS

Wild-Type SecA Expression and Purification. Wild-type, native *E. coli* SecA was expressed and purified as previously described.[16] SecA samples were exchanged by using spin columns in a working buffer containing 20 mM 4-(2-hydroxyethyl)-1-piperazineethanesulfonic acid (HEPES) (pH 7.5), 0.5 mM ethylenediaminetetraacetic acid (EDTA), 0.1 mM tris(2-carboxyethyl)phosphine (TCEP), and 100−500 mM KCl. The SecA concentration was determined by absorbance at 280 nm, using a molar absorptivity (ε_{280}) of 75750 M^{-1} cm^{-1} calculated with Sednterp.[41]

HDX MS Protocol. Given the high sensitivity of SecA dimerization to salt concentration (K_d increases from 0.014 μM at 100 mM KCl to 40.4 μM at 500 mM KCl),[16] this effect was exploited to permit comparison of HDX of the SecA dimer (low salt) and monomer (high salt). Stock solutions of untagged, wild-type SecA were prepared at 6 μM in either low-salt (100 mM KCl) or high-salt (500 mM KCl) pH 7.5 buffer, each containing 20 mM HEPES, 0.5 mM EDTA, and 0.1 mM TCEP. Samples were equilibrated at 25 °C for 1 h before HDX analysis. Continuous labeling with deuterium was initiated by diluting 4 μL of the stock solution into 16 μL of D_2O with an identical KCl concentration. On the basis of the measured dissociation constants, the low-salt samples were 93% dimer and the high-salt samples were 95% monomer. HDX was measured at 10 s, 30 s, 1 min, 2 min, 15 min, 1 h, and 4 h. Two proteases, pepsin and fungal XIII, were used for protein digestion to achieve high peptide coverage. For measurement, the exchange reaction was quenched at various times by mixing with 30 μL of 3 M urea and 1% trifluoroacetic acid (TFA) at ∼1 °C. The mixture was then passed over a custom-packed pepsin column (2 mm × 20 mm) at a rate of 200 μL/min. For fungal XIII digestion, the exchange reaction was quenched with 30 μL of 1.2 mg/mL fungal XIII and 1% formic acid (FA) in water and the mixture placed on ice for 2 min. Prior to liquid chromatography−mass spectrometry analysis, the digested peptides were captured on a 2 mm × 15 mm C8 trap column (Agilent, Santa Clara, CA) and desalted with a 3 min flow at a rate of 200 μL/min (H_2O containing 0.1% TFA). Peptides were then separated by using a 2.1 mm × 50 mm reversed-phase C18 column (1.9 μm Hypersil Gold, Thermo Fisher Scientific, Waltham, MA) with an 11.5 min linear gradient from 4 to 40% CH_3CN in 0.1% FA at a rate of 50 μL/min with a nanoACQUITY UPLC system (Waters, Milford, MA). Protein digestion and peptide separation were conducted in a water−ice bath to minimize back exchange. MS detection was performed on an LTQ-Orbitrap (Thermo Fisher Scientific, Santa Clara, CA) with the following instrument parameters: spray voltage of 4 kV, capillary temperature of 225 °C, capillary voltage of 44 V, and tube lens of 100 V. Data were collected with a mass resolving power of 100000 at m/z 400. Each experiment was conducted in duplicate.

HDX Data Analysis. To identify the products of pepsin or fungal XIII digestions and to provide a list of peptides to be followed during HDX, product ion mass spectra were acquired in a data-dependent mode, with the six most abundant ions from each scan selected for MS/MS. The MS/MS *.raw files were then converted to mzXML files and submitted to MassMatrix for peptide identification.[42] This search was also performed against a decoy (reversed) sequence, and ambiguous identifications were discarded. The final peptide list generated from MassMatrix was output as *.csv files.

The peptide list *.csv files and Thermo *.raw files were then input into HDX workbench[43] to calculate the centroid masses of isotopic envelopes (m) and deuterium level (D%). As described previously,[44] $D\% = \{[m(P) - m(N)]/[m(F) - m(N)]\} \times 100\%$, where $m(P)$ and $m(N)$ are the centroid values of partially deuterated peptide and nondeuterated peptide, respectively. The term $m(F)$ is the calculated mass of the fully exchanged peptide. The retention time window used for calculation of the m of each peptide in each sample was manually inspected and adjusted for accurate calculation of D%, and peptides that showed interference by isotopic peaks from other peptides were discarded. The deuterium level was finally adjusted by dividing the equation given above by 0.8, because the exchange medium had a deuterium content of 80%. The data were not corrected for back exchange because two states were compared.

SecA Mutagenesis. Robetta[45] was used to identify residues lying within potential dimerization interfaces in SecA crystal structures and to guide the selection of residues at which single-alanine substitutions are expected to most strongly destabilize dimerization. The algorithm computes the binding free energies of the wild-type and mutant complexes to afford the destabilization as $\Delta\Delta G = \Delta G_{mutant} - \Delta G_{wild\text{-}type}$. Residues for which $\Delta\Delta G$ is predicted to be >1 kcal/mol within the dimer interfaces were identified from the following SecA crystal structures: *E. coli* (PDB entry 2FSF),[31] *Thermus thermophilus* (PDB entry 2IPC),[29] *B. subtilis* (PDB entry 1M6N),[27] *B. subtilis* (PDB entry 2IBM),[30] and *Mycobacterium tuberculosis* (PDB entry 1NL3).[28] Sequence and structure alignments using BLAST and PDBeFold were performed to map the selected residues onto *E. coli* SecA.

Mutations were introduced by using the QuikChange method as described by the manufacturer (Stratagene/Agilent Technologies, Santa Clara, CA). The SecA mutants contained a C-terminal His_6 tag to facilitate purification without contamination from endogenous, wild-type SecA. The mutants were expressed and purified as described previously.[36]

Analytical Ultracentrifugation. Sedimentation velocity analytical ultracentrifugation measurements were performed using interference optics at 20 °C and 40000 rpm using an An-50 Ti rotor in a Beckman-Coulter XL-I analytical ultracentrifuge. Samples were loaded into synthetic boundary, aluminum-filled Epon cells equipped with sapphire windows. To facilitate analysis of the monomer−dimer equilibrium, sedimentation velocity measurements were performed in 300 mM KCl at 20 °C, where K_d lies in the low micromolar range.[16] Data were initially analyzed by using DCDT+[46] to obtain $g(s^*)$ distributions for visual inspection. Multiple data sets were globally fit using SEDANAL[47] to obtain the monomer−dimer equilibrium constants. Molecular masses, partial specific volumes, solvent densities, and viscosities were calculated by using Sednterp.[41]

Because mutants were generated with a C-terminal His_6 tag, dimerization of wild-type SecA was compared with and without a His_6 tag over a concentration range of 0.5−10 μM in 300 mM KCl by using sedimentation velocity with interference optics. Under these conditions, the dimer dissociation constants of wild-type SecA and SecA containing a C-terminal His_6 tag are

dx.doi.org/10.1021/bi500348p | Biochemistry 2014, 53, 3248−3260

4.3 ± 0.9 and 3.7 ± 0.2 μM, respectively, indicating that the His_6 tag does not significantly affect dimerization.[36]

Normal Mode Analysis. To perform normal mode analysis (NMA) to examine the modal description of the opening and closing transitions, we first had to define the open and closed states of *E. coli* SecA in the monomer and dimer forms. The open monomer form was taken as the structure of *E. coli* SecA determined by NMR (PDB entry 2VDA).[8] A closed monomer form was generated by building a homology model for the *E. coli* sequence based upon the *B. subtilis* X-ray structure (PDB entry 1M6N) using the Chimera[48] interface to Modeler version 9.11.[49] The closed state model (CSM) had an overall structural topology consistent with the 2VDA structure; however, there was a region in NBD II in which the CSM did not reproduce the secondary structural elements present in the 2VDA structure. The long helix-spanning residues 532−553 as well as the short helix-spanning residues 518−525 in 2VDA were unstructured in the CSM. We chose to model these missing helical segments into the CSM, as our purpose was to examine interdomain conformational changes, not intradomain changes. The modeling of the helical segments into the CSM was done by performing a local structural alignment over residues 500−510 and 553−558 between the 2VDA structure and the CSM. The coordinates for residues 515−552 were copied from the 2VDA structure into the CSM, and then the CSM structure was energy minimized for 500 steps using the steepest descent algorithm with harmonic restraints (100 kcal mol^{-1} $Å^{-2}$) on the backbone atoms. The helical segment modeling and energy minimization were performed in CHARMM (version 37a1)[50] using the CHARMM27/CMAP force field.[51,52] Models for the dimer in open and closed states were constructed by aligning the 2VDA and CSM structures with each of the monomers in the 1M6N dimer, using the Chimera MatchMaker tool. The dimer structures had both monomers in open or closed configurations; models with mixed open−closed dimers were not considered.

NMA was performed on four structures: open monomer, closed monomer, open dimer, and closed dimer. The calculations were conducted using ProDy,[53] in which a Cα-based anisotropic network model (ANM)[54] was constructed with harmonic springs between atoms separated by <12 Å. The modes were determined and projected onto the displacement vector describing the structural change between open and closed states (or vice versa). Overlap values were calculated by taking the square of the normalized dot product between the displacement and mode vectors. The ability of a mode to change the separation between the PBD and HWD was quantified by normalizing the modes such that the maximal displacement of any atom was 1 Å. The structures were then displaced by the normalized modes, and the change in the separation between the centers of geometry of the PBD and HWD was calculated.

RESULTS

Analysis of the SecA Dimer Interface by HDX MS. Because the oligomeric state of SecA depends on the KCl concentration, and the intrinsic exchange rate of amide protons is largely unaffected by different salt concentrations,[55] we prepared samples of SecA containing predominantly the monomer or dimer, at the same protein concentration, by simply varying the KCl concentration. Any measured changes in HDX rates would then reliably reflect any dimerization-induced changes in the protein. We previously determined that the K_d for SecA dimerization at 20 °C varies from 0.014 μM at 100 mM KCl to 40.4 μM at 500 mM KCl.[16] We also found that K_d decreases monotonically by a factor of approximately 2 for every 5 °C increase in temperature; thus, at 25 °C, where we conducted HDX, the K_d values of SecA in 100 and 500 mM KCl are approximately 0.007 and 20.2 μM, respectively. For each incubation in our continuous HDX experiments, the SecA stock solution was diluted from 6 to 1.2 μM with D_2O buffer. Under these conditions, 93% of the SecA is dimeric at 100 mM KCl and 95% is monomeric at 500 mM KCl.

To obtain high coverage of SecA in the digestion following HDX, we supplemented the traditional pepsin digestion with a separate one using acidic protease, fungal XIII. Pepsin digestion alone gave 86% coverage; missing were 35 residues at the N-terminus and 30 residues at the C-terminus (Figure S1A of the Supporting Information). Fungal XIII digestion, however, allowed us to recover many peptides covering the N-terminus (Figure S1B of the Supporting Information). Combining the peptides from the two digestions provided high (96%) coverage for the total of 901 amino acid residues in this large protein.

We expect that regions on the protein with defined secondary structures will undergo HDX that is slower than that of unstructured regions or loops because protein backbone amide hydrogen exchange rates are highly dependent on local fluctuations in structure and solvent accessibility.[56] We mapped for visual convenience the HDX results for the SecA monomer onto the NMR structure of *E. coli* SecA (PDB entry 2VDA). The time-dependent deuterium uptake for the SecA peptides from pepsin and fungal XIII digestion, measured at seven time points, was used in the mapping (Figure S2 of the Supporting Information).

In general, the peptides located completely in α-helical or β-sheet regions exhibit slower HDX (<40% at short time points) and are more protected than those at loops and termini. One exception is the peptide covering residues 602−609. Although this region is an α-helix in NBD II, it is dynamic with >70% of the amide hydrogens exchanged after 10 s. Judging from the NMR structure, we see that this helix is located at the periphery of NBD II and is detached from the main body by two loops, imparting greater solvent accessibility and more frequent local conformational fluctuations to this region. Noticeably, the N-terminal peptides covering residues 1−6 and 7−15 were also found to be highly dynamic, with maximal exchange within 10 s. Upon examination of different exchange behavior from 10 s to 4 h, most of the peptides contained within α-helical or β-sheet regions underwent increases of <40%. Interestingly, unlike most others, peptides derived from the long α-helix in HSD covering residues 627−666 showed an increase in the level of deuterium uptake of >80%. This may reflect the relatively higher dynamics of this α-helical region, also named the "transducer helix",[57] which, as indicated by its name, is important for allosteric communication among NBD I, NBD II, the PBD, and the C-domain.[37]

To determine the dimerization interface of SecA, we applied comprehensive differential HDX analysis of the monomer and dimer. In this approach, the HDX kinetics of peptic/fungal peptides derived from the SecA monomer and dimer were compared [all the percentage of deuterium incorporated, D%, vs time (log scale) plots are presented in the Supporting Information (Figures S3 and S4)]. As expected, some regions in the dimer became more protected against exchange than in the monomer. The average differences in D% (ΔD%) for the duplicate analysis of seven exchange time points were

dx.doi.org/10.1021/bi500348p | *Biochemistry* 2014, 53, 3248−3260

calculated, and regions with significant differential deuteration levels are listed in Table 1. The differences between the monomer and dimer in these regions are considered significant because all peptic and fungal peptides covering the same region showed consistent HDX kinetics, smooth curves, and similar ΔD% values. These regions are categorized into two groups: those that show a large difference [ΔD% ≥ 6 (red)] and those that show a small difference [3 < ΔD% ≤ 5 (magenta)]. We realize that this categorization gives a minimal value for the difference because the extent of exchange at some times can be nearly identical even for a region that shows a large difference at other times. This problem is compensated in part by the choice of the small value of 3 as the threshold for distinguishing regions that change upon dimerization. This value, admittedly arbitrary, would distinguish curves that are nearly parallel and modestly separated and curves that show large differences at early time points, for example, and deviate considerably at long times from those that are nearly identical. Those latter regions in SecA have insignificant ΔD% values [<3 (not listed in Table 1)]. The value of 6 distinguishes regions showing small but real changes from those that show large changes. For example, Figure 3D shows some HDX kinetic plots of regions that are unaffected by SecA dimerization. This consistency over most regions in SecA serves as a negative control in showing that the HDX rate is unaffected by KCl concentration and indicates there are large regions of the protein that show little change in HDX upon dimerization.

In contrast, several regions that show significant ΔD% values (Table 1) must have different structures or interactions in monomer and dimer states. The largest differences are observed

Table 1. SecA Peptides Showing Different Levels of Deuterium Incorporation Induced by Dimerization[b]

Region	Domain	Pepsin Digestion		Fungal XIII Digestion	
		Number of peptides	Avg. ΔD%	Number of peptides	Avg. ΔD%
208-216	NBD I	1	3	3	4
313-319	PBD	1	4	1	3
320-338		9	10	4	10
350-374		4	13	5	14
375-380	NBD	3	4	2	5
398-408		3	7	6	6
427-437	NBD II	2	4	3	5
562-574		NA[a]	NA[a]	2	9
575-587		1	5	6	5
626-638	HSD	4	10	6	10
639-671		6	6	4	7
672-690	HWD	2	4	4	4
701-708		5	3	NA[a]	NA[a]
723-737		4	4	3	4
744-757		12	6	3	6
758-774	HSD	5	3	6	3
775-783		4	8	1	8
815-830		4	4	6	4

[a]Not available. [b]The ΔD% values represent the average difference in *D* incorporation across all HDX times for the monomer and dimer. The number of peptides is the number of overlapping peptides covering corresponding regions, all of which show consistent ΔD% values. The red and magenta colors correspond to large (ΔD% ≥ 6) and small (3 < ΔD% ≤ 5) differences, respectively. For a more detailed breakdown of the HDX data, see Figures S3 and S4 of the Supporting Information.

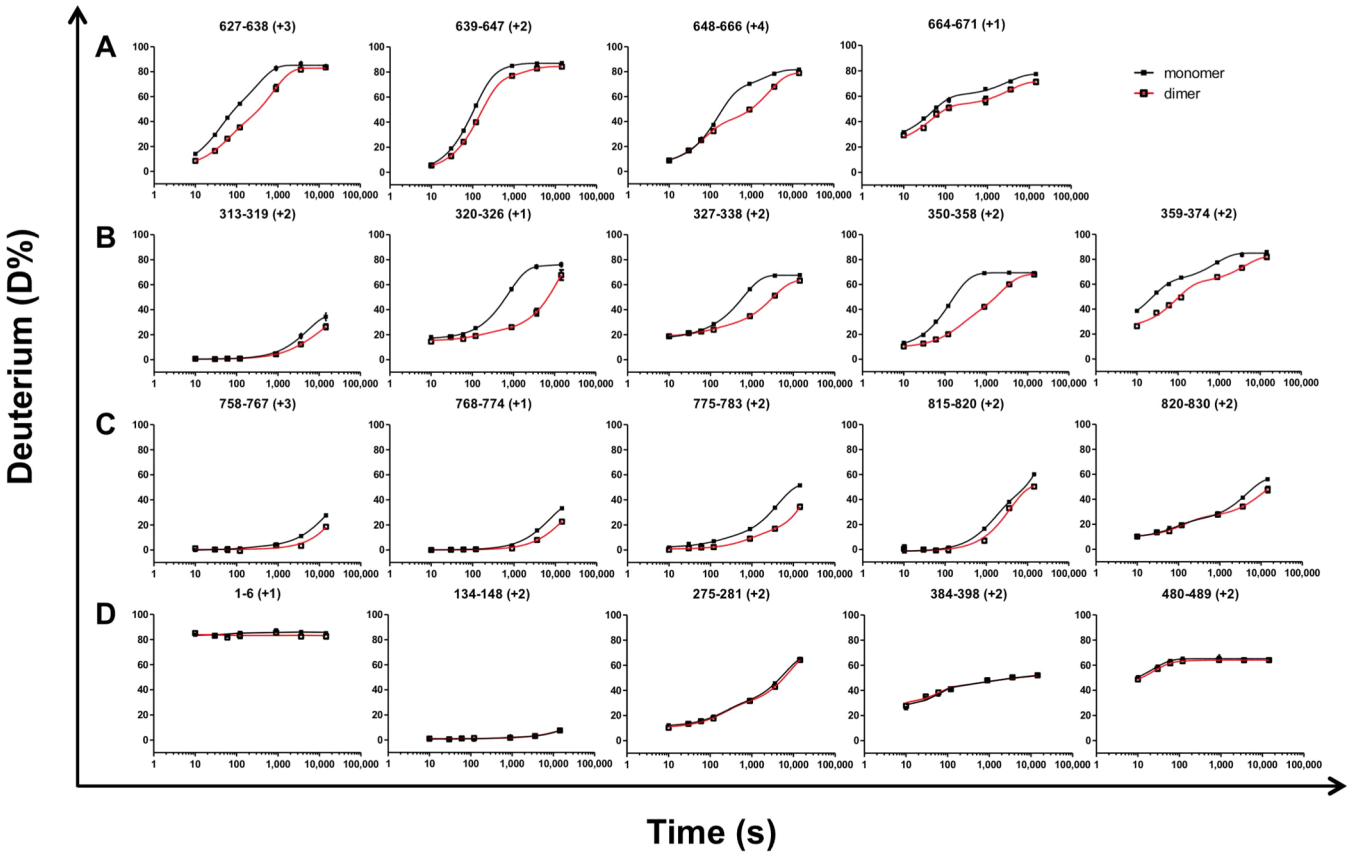

Figure 3. Peptide-level HDX kinetics of SecA. A comparison between the monomer (black) and dimer (red) shows significant changes in HDX at the transducer helix from the HSD (A), regions in the PBD (B), and two helix fingers from HSD (C) and no differences in HDX at regions undergoing little structural change (D). The corresponding regions for panels A–C are marked in Figure 4A.

dx.doi.org/10.1021/bi500348p | *Biochemistry* 2014, 53, 3248–3260

for peptides within the region of residues 627−671 in the HSD (Figure 3A) and within the regions of residues 313−338 and 350−374 in the PBD (Figure 3B). Peptides encompassing residues 758−774 and 815−830 in the HSD show small changes in ΔD%, but a large difference is detected for residues 775−783 (Figure 3C). The kinetic curves for the dimer typically come together at long times with that of the monomer, suggesting that the dimer has a relatively large off rate and allowing the protomer to be freed from the dimer and ultimately to undergo the exchange of the monomer (recall that there is 7% monomer in the solution in which the dimer is largely formed).

To help understand the interface that forms upon SecA dimerization, we mapped the regions identified in Table 1 onto the NMR structure of SecA using the same color code (Figure 4A,B). The three locations exhibiting the greatest difference in

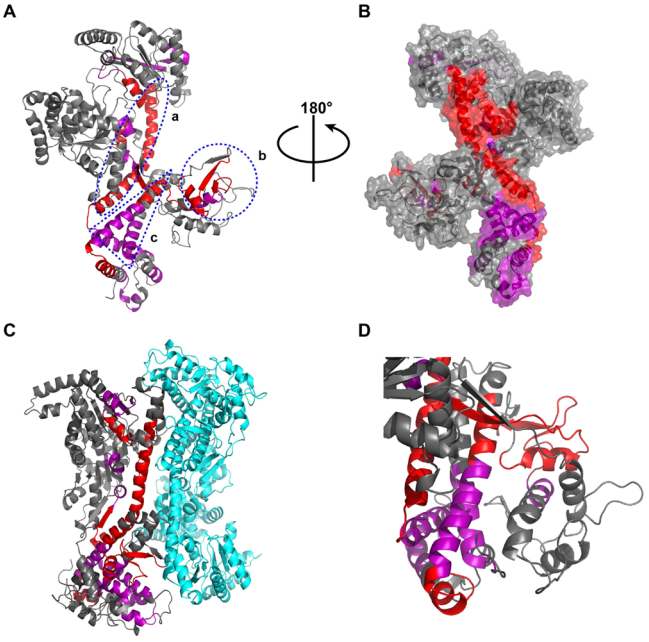

Figure 4. Structural analysis of SecA HDX kinetics. (A and B) Exchange rates mapped onto the *E. coli* SecA (PDB entry 2VDA) structure. Regions exhibiting a large difference (ΔD% ≥ 6) are colored red, and regions exhibiting a small difference (3 < ΔD% ≤ 5) are colored magenta (as in Table 1). (A) Ribbon diagram. Regions denoted a′−c′ correspond to peptides in panels A−C of Figure 3, respectively. (B) Surface representation. (C and D) Exchange rates mapped onto the closed form model of *E. coli* SecA. (C) Dimer structure. The coloring of the left protomer corresponds to that in panels A and B. (D) Interface of the PBD and the C-domain. Generation of the closed form model is described in Materials and Methods.

HDX (Figure 3A−C) are denoted with a′−c′, respectively, on the crystal structure shown in Figure 4A. Region a′ corresponds to the long transducer helix in HSD. Region b′ lies within the PBD and includes two antiparallel β-strands and the following α-helix. Region c′ contains the two-helix finger from the HSD. Other regions within the HWD, NBD I, and NBD II also show some differential ΔD% and are highlighted in Figure 4.

The regions of SecA that show reduced HDX upon dimerization lie on multiple faces of the protomer surface, suggesting that large conformational changes accompany dimerization. Using the crystal structure of 1M6N as a reference, we attribute the decreased HDX in the transducer helix (region a′) to dimer interface formation; this is also consistent with our AUC results described below. We assign the decreased HDX in the PBD (region b′) to an induced allosteric effect caused by dimerization. Corresponding HDX changes are also evident within region c′ and the HWD, supporting a model in which SecA dimerization induces movement of the PBD into a closed conformation where it interacts with the C-terminal portion of SecA. This model is consistent with the previous observation of open and closed conformations of the PBD.[14,27,30,37,38,58,59] In the closed conformation structures, the PBD interacts extensively with the C-terminal domain and forms a compact structure, whereas in the open conformation, the PBD is more solvent-exposed and would, therefore, undergo a greater extent of HDX. Because of its proximity to the transducer helix, the altered HDX in the two-helix finger may arise from dimerization or altered interactions with the PBD. The small ΔD% of the short peptide of residues 427−437 located in NBD II opposite the HSD may be due to an allosteric effect.

Analysis of the SecA Dimer Interface by AUC. To complement our analysis of the dimer interface by HDX, we used AUC to probe the energetic contribution of individual surface residues to SecA dimerization. We chose residues for substitution with alanine using the dimer interfaces observed within the SecA crystal structures from multiple bacterial species.[27−31] Although the SecA fold is largely conserved in these structures, they reveal very different interfaces (Figure 2). We used Robetta[45] to identify residues lying within potential dimerization interfaces and to guide selection of single-alanine substitutions that are expected to strongly destabilize the SecA dimerization. We focused on residues for which Robetta predicts a destabilization of $\Delta\Delta G > 1$ kcal/mol for the interface (Tables S1−S5 of the Supporting Information).[27−31] We chose to characterize SecA dimerization in the context of the *E. coli* protein because its biophysical properties are the most well-characterized.[9,10,16,23,60−75]

Previous studies[20,21,25,76,77] suggested that the N-terminus of SecA is involved in dimerization. The two crystal structures from *B. subtilis* SecA (PDB entry 1M6N)[27] and *T. thermophilus* SecA (PDB entry 2IPC)[29] support these conclusions that the N-termini form part of the dimer interface. We previously found that substitution of N-terminal residues based on the *B. subtilis* 1M6N dimer interface strongly inhibits SecA dimerization. For example, L5A and L6A (*E. coli*) substitutions[36] decrease the level of binding by 3- and 5-fold, respectively, corresponding to a dimer destabilization of 0.6−1 kcal/mol (Table 2). These effects follow the trend but are somewhat smaller than those predicted by Robetta for the antiparallel *B. subtilis* dimer interface [PDB entry 1M6N (Table S3 of the Supporting Information)].

The *T. thermophilus* SecA dimer interface (PDB entry 2IPC) contains two salt bridges, R732−D675 and R736−E742, that may contribute to stabilization.[29] Robetta predicts that substitution of these residues with alanine should destabilize the dimer by at least 1 kcal/mol (Table S2 of the Supporting Information). Substitution of the corresponding *E. coli* residues with alanine (D568A, K625A, N629A, and E635A), however, does not significantly affect the SecA dimerization affinity (Table 2). However, it should be noted that one of the salt bridge residues (R736) is not conserved in *E. coli* (N629). Furthermore, the Q801A (*E. coli*) substitution also has little effect on the dimerization, as its K_d value is similar to that of

dx.doi.org/10.1021/bi500348p | *Biochemistry* 2014, 53, 3248−3260

Table 2. Dimer Dissociation Constants of Single-Alanine Substitution Mutants of SecA

residue	K_d (μM)	ΔG^a (kcal/mol)	$\Delta\Delta G^b$ (kcal/mol)
wild-type[c]	3.7 ± 0.2	−7.29 ± 0.03	0
L5[c]	11.0 ± 2.2	−6.65 ± 0.12	0.64
L6[c]	19.5 ± 4.8	−6.31 ± 0.14	0.98
K8	8.6 ± 0.5	−6.79 ± 0.03	0.50
R342	3.7 ± 0.2	−7.28 ± 0.03	0.01
D568	4.8 ± 0.8	−7.14 ± 0.09	0.15
K625	2.7 ± 2.4	−7.47 ± 0.44	−0.18
N629	2.3 ± 0.4	−7.55 ± 0.09	−0.26
K633	3.6 ± 0.1	−7.30 ± 0.02	−0.01
E635	2.3 ± 0.8	−7.56 ± 0.19	−0.27
D640	1.6 ± 0.01	−7.78 ± 0.005	−0.49
Q662	0.10 ± 0.01	−9.38 ± 0.06	−2.09
E665	12.7 ± 0.3	−6.57 ± 0.01	0.72
K800	3.2 ± 0.3	−7.37 ± 0.05	−0.08
Q801	2.6 ± 0.3	−7.48 ± 0.06	−0.19
E802	3.3 ± 0.3	−7.35 ± 0.05	−0.05
F811	2.3 ± 0.1	−7.56 ± 0.03	−0.27
L815	2.2 ± 0.03	−7.58 ± 0.01	−0.29
L818	3.4 ± 0.1	−7.33 ± 0.02	−0.04

[a] $\Delta G = RT \ln K_d$. [b] $\Delta\Delta G = \Delta G_{mutant} - \Delta G_{wild\text{-}type}$. [c] Previously reported in ref 36.

wild-type SecA. This is in contrast to substitutions of the corresponding residue (R750) in *B. subtilis* that cause monomerization of SecA.[20,25,30]

On the basis of the results described above, we selected additional residues derived from the *B. subtilis* SecA dimer interface (PDB entry 1M6N) according to the following criteria: (1) residues interacting with the N-terminus (E665, F811, L815, and L818), (2) those commonly located at interfaces (R342), (3) those creating salt bridges (K8−E665, D640−K800, and K633−E802), and (4) residues found to lie in several alternative interfaces (K8 and K633). Of these, we found two residues at which alanine substitution significantly affected SecA dimerization: K8 and E665 (Table 2). Global analysis of SecA E665A dimerization in 300 mM KCl (Figure 5) yields a dimer K_d of 12.6 ± 0.3 μM, indicating that the E665A substitution induces a 3.5-fold reduction in dimerization affinity ($\Delta\Delta G$ = 0.72 kcal/mol). The Q662A substitution strongly enhances dimerization, decreasing K_d by 36-fold ($\Delta\Delta G$ = −2.1 kcal/mol), although Robetta predicts that this mutation should moderately destabilize dimerization by ∼0.5 kcal/mol (Table S3 of the Supporting Information). The locations of the single-alanine mutations that affect SecA dimerization are indicated in Figure 6.

Because we found that N-terminal residues are important for dimerization, we analyzed this region in greater detail. Some

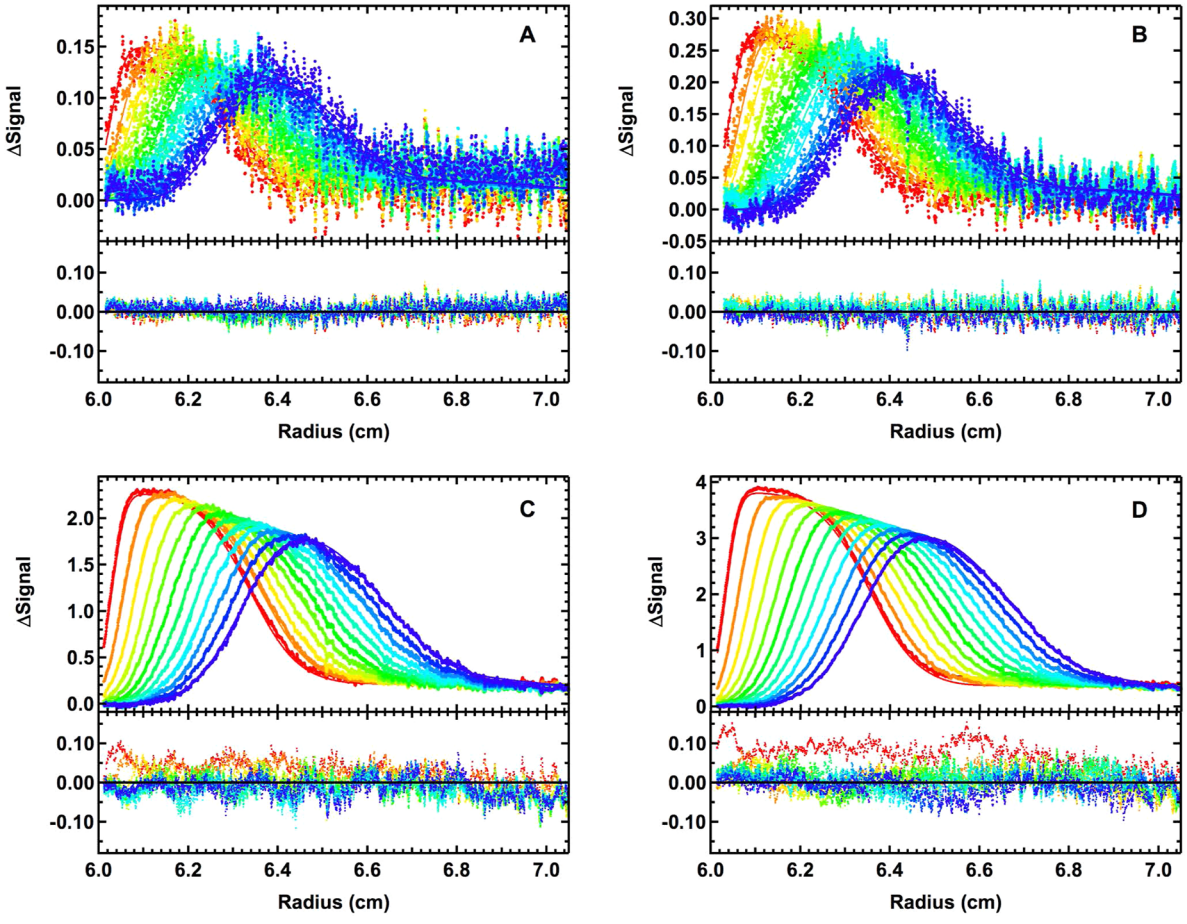

Figure 5. Sedimentation velocity analysis of SecA E665A self-association in 300 mM KCl. Global analysis of sedimentation velocity difference curves obtained with interference optics. The data were subtracted in pairs to remove the time-independent noise. SecA E665A concentrations of (A) 0.5, (B) 1, (C) 5, and (D) 10 μM. Conditions: rotor speed, 40000 rpm; temperature, 20 °C. The data were fit to a monomer−dimer equilibrium plus incompetent tetramer model. The best-fit K_d = 12.8 ± 0.5 μM with a root-mean-square deviation of 0.017 fringe.

dx.doi.org/10.1021/bi500348p | *Biochemistry* 2014, 53, 3248−3260

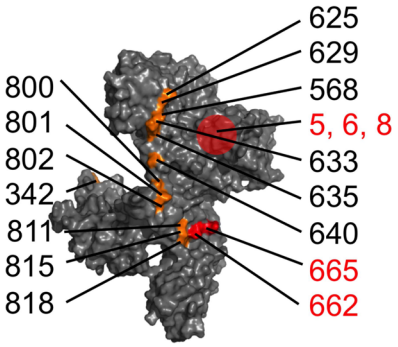

Figure 6. Single-alanine substitution mutants. Residues selected for alanine substitution are mapped on the *E. coli* SecA (PDB entry 2VDA)[8] structure. Residues that affect dimerization are colored red, while those that are neutral are colored orange. Residues 5, 6, and 8 were not resolved in this structure and are denoted with a red circle.

studies using deletion constructs suggested that the N-terminus is part of the SecA dimerization interface,[20,21,25,76,77] whereas others concluded the opposite.[78,79] To address this issue, we deleted residues 2−8, 2−9, and 2−10 (Δ2−8, Δ2−9, and Δ2−10, respectively) from wild-type SecA and examined the effects on dimerization. SecA dimerization affinity decreases with the number of residues deleted from the N-terminus (Table 3). Deleting residues 2−8 decreased K_d by 5-fold (∼1 kcal/mol), whereas deleting residues 2−10 decreased K_d by 27-fold (∼1.9 kcal/mol).

It is possible that the N-terminal deletion mutants form a dimer interface different from that of wild-type SecA. The *E. coli* structure (PDB entry 2FSF)[31] was determined using SecA lacking residues 2−8, whereas the SecA construct used for the antiparallel *B. subtilis* structure (PDB entry 1M6N)[27] contains residues 2−8. These differences may explain the different interfaces observed in these structures (Figure 2).

To further probe the nature of the interactions at the N-terminus without introducing deletions, we also generated SecA constructs containing multiple alanine substitutions at the N-terminus. Noting that residues 2−10 (LIKLLTKVF) are mostly hydrophobic, we created multiple alanine substitutions of the hydrophobic residues in this region. We simultaneously substituted four (L2A/I3A/L5A/L6A) and five (L2A/I3A/L5A/L6A/V9A and I3A/L5A/L6A/V9A/F10A) residues at the N-terminus with alanine and analyzed SecA dimerization in 300 mM KCl. We found that dimerization affinity decreases as additional alanine substitutions are introduced, such that with five alanine substitutions, no dimerization occurs (Table 3). If the alanine substitution and deletion mutants had the same dimer interfaces, the dimerization of SecA Δ2−8 would be weaker than, if not similar to, that of SecA L2A/I3A/L5A/L6A. We observed, however, that dimerization of SecA L2A/I3A/L5A/L6A is 3-fold weaker than that of SecA Δ2−8. This result suggests that the dimer interfaces of these constructs may be different, assuming that alanine substitutions at the N-terminus do not cause greater destabilization of the dimer interaction than deletion. We also determined the role of hydrophilic residues at the N-terminus using SecA K4Q/K8Q. These substitutions have an impact on SecA dimerization similar to that of K8A but have an impact smaller than that of the hydrophobic substitutions (Table 3).

Normal Mode Analysis. To explore the possibility of an allosteric mechanism in which SecA dimerization mediates structural changes, we performed normal mode analysis on the monomer and dimer in the open and closed states. Normal mode analysis is a structure-based method for understanding how the dynamics of proteins are encoded by the structure.[80] For many large macromolecular complexes, it has been shown that the displacements required for a system to undergo a transition between states can be described by a few normal modes.[81−84] Furthermore, it is the low-frequency modes, which are related to the large scale, collective motions, that typically describe large conformational changes.

Figure 7 shows the projection of the normal modes onto the displacement vector describing the structural differences between the open (PDB entry 2VDA) and closed (homology model based upon PDB entry 1M6N) states of *E. coli* SecA for both the monomer and the dimer. The structural difference between the open and closed states for the monomer is shown in Figure 7B. It can be seen that the major change is related to the separation between the PBD and HWD regions. What we can observe from Figure 7A is that the open to closed transition is more robustly described by the low-frequency modes than the closed to open transition, indicating that the closing transition requires less energy (lower-frequency modes) than the opening transition. When we compare the dimer and monomer closing transitions, the dimer has slightly larger projections, indicating the transition for the dimer requires less energy. Interestingly, this trend is reversed for the opening transition, wherein the monomer has larger projections (takes less energy) than the dimer. These results point toward the energy landscape, in the opening direction, to be steeper (i.e., deeper well) for the dimer than for the monomer (i.e., the closed configuration of the dimer is stabilized). In Figure 7C, we focus our attention on the low-frequency end of the mode spectrum, and the ability of these modes to change the separation between the PBD and HWD. We observe that the dimer has a mode that couples much more strongly to the PBD−HWD domain separation than any mode in the monomer. That mode (mode 7) is shown as a porcupine plot in Figure 7D, displaying those residues that have the most

Table 3. Dimer Dissociation Constants of N-Terminal Mutants of SecA

SecA mutant	K_d (μM)	ΔG^a (kcal/mol)	$\Delta\Delta G^b$ (kcal/mol)
Δ2−8	20.3 ± 1.0	−6.29 ± 0.03	1.00
Δ2−9	17.1 ± 1.2	−6.39 ± 0.04	0.90
Δ2−10	97.5 ± 18.7	−5.38 ± 0.11	1.91
L2A/I3A/L5A/L6A	62.0 ± 7.0	−5.64 ± 0.07	1.65
L2A/I3A/L5A/L6A/V9A	ND[c]	–	–
I3A/L5A/L6A/V9A/F10A	ND[c]	–	–
K4Q/K8Q	9.2 ± 0.7	−6.75 ± 0.05	0.54

[a] $\Delta G = RT \ln K_d$. [b] $\Delta\Delta G = \Delta G_{mutant} - \Delta G_{wild\text{-}type}$. [c] Dimerization was not detectable.

dx.doi.org/10.1021/bi500348p | *Biochemistry* 2014, 53, 3248−3260

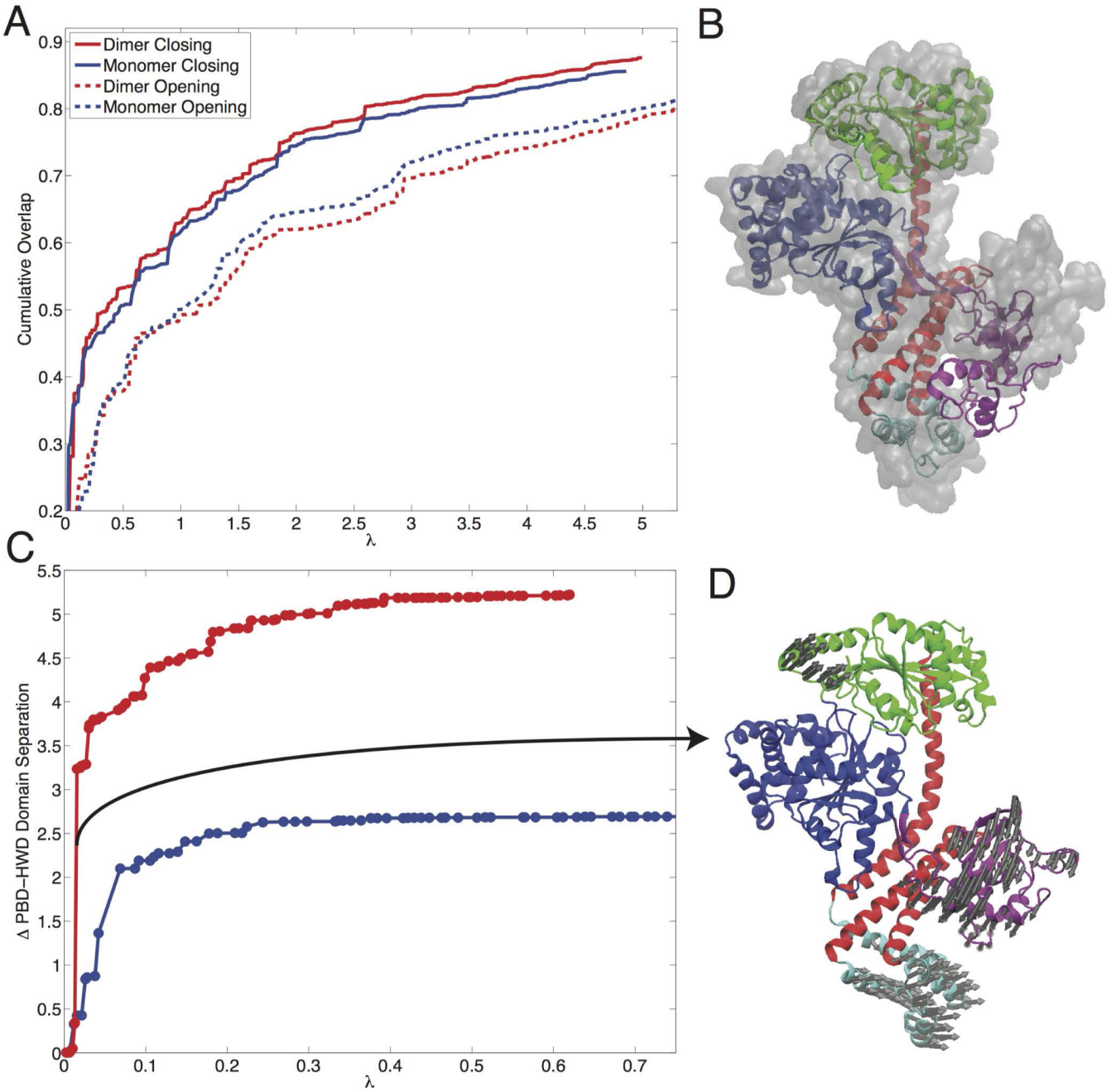

Figure 7. Normal mode analysis of SecA monomer and proposed dimer configurations. (A) Normal modes are calculated for the open and closed states for both the dimer and the monomer. The cumulative overlaps (normalized squared dot product) of the modes onto the displacement vector are shown for the slowest 20% of the mode spectra. λ is the eigenvalue of each normal mode. (B) The open state (PDB entry 2VDA) is shown as a surface representation in gray, and the modeled closed state is shown as a red ribbon. (C) The slowest 100 modes were examined to detect their ability to change the PBD−HWD separation distance. (D) Mode 7 from the open dimer structure is shown as a porcupine plot (mapped onto the open monomer for the sake of clarity), where the arrow lengths represent the relative magnitudes of displacement. The arrows on residues with small displacements were removed to highlight the most dynamic regions.

significant displacements. The presence of this mode, which does not appear (as a single mode) in the monomer, indicates our proposed dimer interface is influencing the global dynamics of SecA and providing flexibility to the PBD and HWD regions of the structure. These regions are distal to the proposed dimer interface, and this observation is consistent with an allosteric mechanism in which dimerization is linked to an open to closed transition. The results from normal mode analysis are consistent with the regions that undergo protection from HDX in the dimer state.

DISCUSSION

In this study, we utilized complementary experimental approaches, HDX MS and site-directed mutagenesis with AUC, to probe the dimer interface of SecA in solution. HDX examines the effects of dimerization based on changes in peptide backbone solvent accessibility, with spatial resolution limited by digestion coverage and peptide size, whereas site-directed mutagenesis with AUC measures the energetic contributions of individual residues to dimerization. The

dx.doi.org/10.1021/bi500348p | *Biochemistry* 2014, 53, 3248−3260

HDX measurements were performed with a limited (10 s) time resolution and are, thus, insensitive to faster processes.

The HDX MS and AUC data together indicate that the HSD is a component of the dimer interface. Site-directed mutagenesis with AUC shows that residues Q662 and E665 lying at the C-terminus of the long transducer helix in the HSD are involved in dimerization. The HDX results implicate a larger region within the HSD, including the entire transducer helix and the two-helix finger. The difference in the extent of HSD involvement in the dimer interface detected by these methods may arise because some of the interfacial residues do not provide a large energetic contribution to dimerization. Alternatively, the transducer helix is known to be mobile,[37] and changes in the accessibility of this helix upon dimerization may be communicated to regions lying distal from the dimer interface. With the exception of the *E. coli* structure (PDB entry 2FSF), each of the SecA crystal structures includes N-terminal portions of the transducer helix within the dimer interface (Figure 2). However, only the *B. subtilis* 1M6N interface also encompasses the C-terminal region of this helix identified by AUC.

The AUC data indicate that the N-terminus contributes to the SecA dimer interface, whereas HDX does not detect differences in this region between the monomer and dimer states. This discrepancy is likely associated with the flexible nature of the N-terminus. In this region, the deuterium uptake reaches a maximum at the shortest exchange time point (10 s), precluding detection of an interface by HDX (Figure S4 of the Supporting Information), consistent with high on and off rates for the interaction. Our data demonstrating the involvement of the N-terminus in the SecA dimer interface disagree with three dimer structures (PDB entries 2FSF, 1NL3, and 2IBM) that do not include the N-terminus as part of the dimer interface. Note that these three structures were determined using SecA deletion mutants. Specifically, the *E. coli* SecA (PDB entry 2FSF) structure was determined using an N-terminal deletion mutant (residues 9−861). In contrast, the dimer interfaces from *T. thermophilus* (PDB entry 2IPC) and *B. subtilis* (PDB entry 1M6N) structures contain the N-terminus.

Overall, the HDX and AUC data appear to be most consistent with the *B. subtilis* SecA 1M6N antiparallel dimer arrangement.[27] However, only five of 14 alanine substitutions predicted to diminish dimerization affinity based on the 1M6N interface actually reduced the level of dimerization of *E. coli* SecA, despite the 50% identical sequences of these orthologs. This discrepancy may indicate that the solution interface dimer is similar, but not identical, to that found in the 1M6N structure, and thus, none of the crystal structures may correspond to the interface adopted by cytoplasmic SecA. Alternatively, it was recently reported that SecA adopts multiple dimeric interfaces during translocation,[85] and these may exist in equilibrium in solution. Both proposed dimer interfaces, based on the 1M6N structure and an interface found in the *M. tuberculosis* 1NL3 crystal form (but different from that depicted in Figure 2E), include the N-terminal region and portions of the HSD and HWD. However, the latter interface does not include residues Q662 and E665 that we found to affect SecA dimerization or the N-terminal portions of the transducer helix that are protected from HDX by dimerization. In agreement with our results, interprotomer distances derived from fluorescence resonance energy transfer measurements are also most consistent with the 1M6N interface.[34,35]

The HDX data also reveal that dimerization induces movement of the PBD into a closed conformation where it interacts with the HWD. Normal mode analysis supports such an allosteric mechanism in which dimerization is linked to an open to closed transition. We identified a low-frequency mode in the dimer but not in the monomer that is coupled to the PBD−HWD separation. Consistent with correlation of SecA dimerization with a closing transition of the PBD, *B. subtilis* SecA adopts an open conformation in a monomeric crystal form (PDB entry 1TF5),[38] whereas closed forms are found in two dimeric crystal forms of the same enzyme.[27,30] Cryo-electron microscopy analysis of dimeric *E. coli* SecA reveals a closed state.[14] However, this correlation is not always observed, as a monomeric complex of *Thermotoga maritima* SecA with ADP can be crystallized in a closed state[37] and a crystal structure of dimeric *E. coli* SecA (PDB entry 2FSF) reveals an open state.[31] Crystal packing forces may influence the conformation of the PBD. Consistent with a low barrier for this transition, solution NMR suggests that dimeric SecA rapidly interconverts between a closed state and a predominant open state.[8] Förster resonance energy transfer measurements indicate that signal peptide binding induces dimeric SecA to adopt a more open conformation.[35] Binding of a non-signal sequence peptide in the groove between PBD and NBD II results in the rotation of the PBD toward NBD II,[37] and interaction of SecA with SecYEG induces further movement of the PBD to close the clamp.[24]

Our analysis can be interpreted in the context of the closed state model of the *E. coli* SecA dimer based on the 1M6N structure (Figure 4C). The dimer interface is primarily contributed by the HSD and the N-terminus, two regions that lie on the same side of the protomer. The C-terminal domain regions that form an interface with the PBD become less dynamic upon dimerization (Figure 4D). However, the corresponding colored regions in the PBD are not in close contact with the C-terminal domain. Most of the colored residues in the PBD are also removed from the interprotomer interface; however, a short loop does contribute to dimerization [residues 338−342 (Table S3 of the Supporting Information)], and a portion of the reduced HDX in the PBD may be directly associated with dimerization. The two regions in the PBD making close contact with the C-terminal domain, residues 263−268 (loop) and 304−314 (α helix), do not show significant ΔD% between the monomer and dimer. The region of residues 263−268 is a flexible loop that reaches 60% deuterium exchange at the shortest HDX time point, 10 s, and 80% at 4 h (Figure S4 of the Supporting Information). In contrast, the helix in the region of residues 306−314 is rigid and shows <5% deuterium exchange at the longest HDX time point, 4 h (Figure S3 of the Supporting Information). Thus, the absence of a detectable difference in monomer and dimer HDX for these regions can be ascribed to very fast and very slow exchange, respectively, that lie outside the time resolution of this study.

Several studies show that SecA is dimeric when driving translocation of preprotein across SecYEG,[15,19,20,37,77,86] whereas others report that the functional form of SecA is monomeric.[18,24,25] Regions within the PBD and C-domain of SecA interact with the C-terminal region of SecY.[24] When SecA binds to SecYEG, the PBD moves away from the HWD and closer to NBD II.[24] The *B. subtilis* (PDB entry 1M6N) dimer interface supported by the data presented here does not overlap with the SecA−SecYEG interface, so that the intact dimer could

interact with SecYEG. Interaction with SecYEG and subsequent ATP hydrolysis may induce SecA dimer dissociation during the translocation cycle.[1,85] In this context, the movement of the PBD to an open conformation upon SecA dimer dissociation may facilitate transfer of the preprotein to the SecY pore.

CONCLUSIONS

Our data indicate that the SecA dimer interface encompasses portions of the helical scaffold domain, including the long transducer helix, and the N-terminus. These results agree most closely with the dimer interface observed in the 1M6N crystal structure of *B. subtilis* SecA.[27] Additional regions are protected from HDX upon dimerization because of the closure of the PBD−HWD groove. Normal mode analysis supports an allosteric mechanism in which dimerization is linked to an open to closed transition.

ASSOCIATED CONTENT

Supporting Information

Peptide coverage map for pepsin digestion and fungal XIII digestion (Figure S1), dynamics of the SecA monomer (Figure S2), HDX kinetics of SecA peptic peptides (Figure S3), HDX kinetics of SecA fungal peptides (Figure S4), and sedimentation velocity analysis of SecA Q662A self-association in 300 mM KCl (Figure S5). This material is available free of charge via the Internet at http://pubs.acs.org.

AUTHOR INFORMATION

Corresponding Author

*Department of Molecular and Cell Biology, 91 N. Eagleville Rd., U-3125, University of Connecticut, Storrs, CT 06269. E-mail: james.cole@uconn.edu. Phone: (860) 486-4333. Fax: (860) 486-4331.

Author Contributions

A.J.W. and Y.Y. contributed equally to this work.

Funding

The National Institute of General Medical Sciences supported the preparation of SecA and the AUC measurements (GM037639 to D.A.K.) and HDX MS experiments (8 P41 GM103422-36 to M.L.G.).

Notes

The authors declare no competing financial interest.

ACKNOWLEDGMENTS

We thank Ping Zhao for generating some of the SecA mutants.

ABBREVIATIONS

AUC, analytical ultracentrifugation; CTL, C-terminal linker; HDX, hydrogen/deuterium exchange; HSD, helical scaffold domain; HWD, helical wing domain; MS, mass spectrometry; NBD, nucleotide binding domain; NMA, normal mode analysis; PBD, preprotein binding domain; PDB, Protein Data Bank.

REFERENCES

(1) Kusters, I., and Driessen, A. J. (2011) SecA, a remarkable nanomachine. *Cell. Mol. Life Sci. 68*, 2053−2066.

(2) Segers, K., and Anne, J. (2011) Traffic jam at the bacterial sec translocase: Targeting the SecA nanomotor by small-molecule inhibitors. *Chem. Biol. 18*, 685−698.

(3) Economou, A., and Wickner, W. (1994) SecA promotes preprotein translocation by undergoing ATP-driven cycles of membrane insertion and deinsertion. *Cell 78*, 835−843.

(4) Papanikou, E., Karamanou, S., and Economou, A. (2007) Bacterial protein secretion through the translocase nanomachine. *Nat. Rev. Microbiol. 5*, 839−851.

(5) Tomkiewicz, D., Nouwen, N., van Leeuwen, R., Tans, S., and Driessen, A. J. (2006) SecA supports a constant rate of preprotein translocation. *J. Biol. Chem. 281*, 15709−15713.

(6) van der Wolk, J. P., de Wit, J. G., and Driessen, A. J. (1997) The catalytic cycle of the *Escherichia coli* SecA ATPase comprises two distinct preprotein translocation events. *EMBO J. 16*, 7297−7304.

(7) Sardis, M. F., and Economou, A. (2010) SecA: A tale of two protomers. *Mol. Microbiol. 76*, 1070−1081.

(8) Gelis, I., Bonvin, A. M., Keramisanou, D., Koukaki, M., Gouridis, G., Karamanou, S., Economou, A., and Kalodimos, C. G. (2007) Structural basis for signal-sequence recognition by the translocase motor SecA as determined by NMR. *Cell 131*, 756−769.

(9) Musial-Siwek, M., Rusch, S. L., and Kendall, D. A. (2007) Selective photoaffinity labeling identifies the signal peptide binding domain on SecA. *J. Mol. Biol. 365*, 637−648.

(10) Auclair, S. M., Moses, J. P., Musial-Siwek, M., Kendall, D. A., Oliver, D. B., and Mukerji, I. (2010) Mapping of the signal peptide-binding domain of *Escherichia coli* SecA using Forster resonance energy transfer. *Biochemistry 49*, 782−792.

(11) Grady, L. M., Michtavy, J., and Oliver, D. B. (2011) Characterization of the *Escherichia coli* SecA signal peptide-binding site. *J. Bacteriol. 194*, 307−316.

(12) Bhanu, M. K., Zhao, P., and Kendall, D. A. (2013) Mapping of the SecA signal peptide binding site and dimeric interface by using the substituted cysteine accessibility method. *J. Bacteriol. 195*, 4709−4715.

(13) Woodbury, R. L., Hardy, S. J., and Randall, L. L. (2002) Complex behavior in solution of homodimeric SecA. *Protein Sci. 11*, 875−882.

(14) Chen, Y., Pan, X., Tang, Y., Quan, S., Tai, P. C., and Sui, S. F. (2008) Full-length *Escherichia coli* SecA dimerizes in a closed conformation in solution as determined by cryo-electron microscopy. *J. Biol. Chem. 283*, 28783−28787.

(15) Kusters, I., van den Bogaart, G., Kedrov, A., Krasnikov, V., Fulyani, F., Poolman, B., and Driessen, A. J. (2011) Quaternary structure of SecA in solution and bound to SecYEG probed at the single molecule level. *Structure 19*, 430−439.

(16) Wowor, A. J., Yu, D., Kendall, D. A., and Cole, J. L. (2011) Energetics of SecA dimerization. *J. Mol. Biol. 408*, 87−98.

(17) Kimura, E., Akita, M., Matsuyama, S., and Mizushima, S. (1991) Determination of a region in SecA that interacts with presecretory proteins in *Escherichia coli*. *J. Biol. Chem. 266*, 6600−6606.

(18) Or, E., Navon, A., and Rapoport, T. (2002) Dissociation of the dimeric SecA ATPase during protein translocation across the bacterial membrane. *EMBO J. 21*, 4470−4479.

(19) de Keyzer, J., van der Sluis, E. O., Spelbrink, R. E., Nijstad, N., de Kruijff, B., Nouwen, N., van der Does, C., and Driessen, A. J. (2005) Covalently dimerized SecA is functional in protein translocation. *J. Biol. Chem. 280*, 35255−35260.

(20) Jilaveanu, L. B., and Oliver, D. (2006) SecA dimer cross-linked at its subunit interface is functional for protein translocation. *J. Bacteriol. 188*, 335−338.

(21) Wang, H., Na, B., Yang, H., and Tai, P. C. (2008) Additional *in vitro* and *in vivo* evidence for SecA functioning as dimers in the membrane: Dissociation into monomers is not essential for protein translocation in *Escherichia coli*. *J. Bacteriol. 190*, 1413−1418.

(22) Benach, J., Chou, Y. T., Fak, J. J., Itkin, A., Nicolae, D. D., Smith, P. C., Wittrock, G., Floyd, D. L., Golsaz, C. M., Gierasch, L. M., and Hunt, J. F. (2003) Phospholipid-induced monomerization and signal-peptide-induced oligomerization of SecA. *J. Biol. Chem. 278*, 3628−3638.

(23) Musial-Siwek, M., Rusch, S. L., and Kendall, D. A. (2005) Probing the affinity of SecA for signal peptide in different environments. *Biochemistry 44*, 13987−13996.

(24) Zimmer, J., Nam, Y., and Rapoport, T. A. (2008) Structure of a complex of the ATPase SecA and the protein-translocation channel. *Nature 455*, 936−943.
(25) Or, E., Boyd, D., Gon, S., Beckwith, J., and Rapoport, T. (2005) The bacterial ATPase SecA functions as a monomer in protein translocation. *J. Biol. Chem. 280*, 9097−9105.
(26) Or, E., and Rapoport, T. (2007) Cross-linked SecA dimers are not functional in protein translocation. *FEBS Lett. 581*, 2616−2620.
(27) Hunt, J. F., Weinkauf, S., Henry, L., Fak, J. J., McNicholas, P., Oliver, D. B., and Deisenhofer, J. (2002) Nucleotide control of interdomain interactions in the conformational reaction cycle of SecA. *Science 297*, 2018−2026.
(28) Sharma, V., Arockiasamy, A., Ronning, D. R., Savva, C. G., Holzenburg, A., Braunstein, M., Jacobs, W. R., Jr., and Sacchettini, J. C. (2003) Crystal structure of *Mycobacterium tuberculosis* SecA, a preprotein translocating ATPase. *Proc. Natl. Acad. Sci. U.S.A. 100*, 2243−2248.
(29) Vassylyev, D. G., Mori, H., Vassylyeva, M. N., Tsukazaki, T., Kimura, Y., Tahirov, T. H., and Ito, K. (2006) Crystal structure of the translocation ATPase SecA from *Thermus thermophilus* reveals a parallel, head-to-head dimer. *J. Mol. Biol. 364*, 248−258.
(30) Zimmer, J., Li, W., and Rapoport, T. A. (2006) A novel dimer interface and conformational changes revealed by an X-ray structure of *B. subtilis* SecA. *J. Mol. Biol. 364*, 259−265.
(31) Papanikolau, Y., Papadovasilaki, M., Ravelli, R. B., McCarthy, A. A., Cusack, S., Economou, A., and Petratos, K. (2007) Structure of dimeric SecA, the *Escherichia coli* preprotein translocase motor. *J. Mol. Biol. 366*, 1545−1557.
(32) Carugo, O., and Argos, P. (1997) Protein-protein crystal-packing contacts. *Protein Sci. 6*, 2261−2263.
(33) Xu, Q., Canutescu, A. A., Wang, G., Shapovalov, M., Obradovic, Z., and Dunbrack, R. L., Jr. (2008) Statistical analysis of interface similarity in crystals of homologous proteins. *J. Mol. Biol. 381*, 487−507.
(34) Ding, H., Hunt, J. F., Mukerji, I., and Oliver, D. (2003) *Bacillus subtilis* SecA ATPase exists as an antiparallel dimer in solution. *Biochemistry 42*, 8729−8738.
(35) Auclair, S. M., Oliver, D. B., and Mukerji, I. (2013) Defining the solution state dimer structure of *Escherichia coli* SecA using Forster resonance energy transfer. *Biochemistry 52*, 2388−2401.
(36) Yu, D., Wowor, A. J., Cole, J. L., and Kendall, D. A. (2013) Defining the *Escherichia coli* SecA Dimer Interface Residues through *in Vivo* Site-specific Photo-crosslinking. *J. Bacteriol. 195*, 2817−2825.
(37) Zimmer, J., and Rapoport, T. A. (2009) Conformational Flexibility and Peptide Interaction of the Translocation ATPase SecA. *J. Mol. Biol. 394*, 606−612.
(38) Osborne, A. R., Clemons, W. M., Jr., and Rapoport, T. A. (2004) A large conformational change of the translocation ATPase SecA. *Proc. Natl. Acad. Sci. U.S.A. 101*, 10937−10942.
(39) Erlandson, K. J., Miller, S. B., Nam, Y., Osborne, A. R., Zimmer, J., and Rapoport, T. A. (2008) A role for the two-helix finger of the SecA ATPase in protein translocation. *Nature 455*, 984−987.
(40) Gold, V. A., Whitehouse, S., Robson, A., and Collinson, I. (2013) The dynamic action of SecA during the initiation of protein translocation. *Biochem. J. 449*, 695−705.
(41) Laue, T. M., Shah, B., Ridgeway, T. M., and Pelletier, S. L. (1992) Computer-aided interpretation of sedimentation data for proteins. In *Analytical Ultracentrifugation in Biochemistry and Polymer Science* (Harding, S. E., Horton, J. C., and Rowe, A. J., Eds.) pp 90−125, Royal Society of Chemistry, Cambridge, England.
(42) Xu, H., and Freitas, M. A. (2009) MassMatrix: A database search program for rapid characterization of proteins and peptides from tandem mass spectrometry data. *Proteomics 9*, 1548−1555.
(43) Pascal, B. D., Willis, S., Lauer, J. L., Landgraf, R. R., West, G. M., Marciano, D., Novick, S., Goswami, D., Chalmers, M. J., and Griffin, P. R. (2012) HDX workbench: Software for the analysis of H/D exchange MS data. *J. Am. Soc. Mass Spectrom. 23*, 1512−1521.
(44) Zhang, Z., and Smith, D. L. (1993) Determination of amide hydrogen exchange by mass spectrometry: A new tool for protein structure elucidation. *Protein Sci. 2*, 522−531.
(45) Kortemme, T., Kim, D. E., and Baker, D. (2004) Computational alanine scanning of protein-protein interfaces. *Sci. STKE 2004*, pl2.
(46) Philo, J. S. (2006) Improved methods for fitting sedimentation coefficient distributions derived by time-derivative techniques. *Anal. Biochem. 354*, 238−246.
(47) Stafford, W. F., and Sherwood, P. J. (2004) Analysis of heterologous interacting systems by sedimentation velocity: Curve fitting algorithms for estimation of sedimentation coefficients, equilibrium and kinetic constants. *Biophys. Chem. 108*, 231−243.
(48) Pettersen, E. F., Goddard, T. D., Huang, C. C., Couch, G. S., Greenblatt, D. M., Meng, E. C., and Ferrin, T. E. (2004) UCSF Chimera: A visualization system for exploratory research and analysis. *J. Comput. Chem. 25*, 1605−1612.
(49) Sali, A., and Blundell, T. L. (1993) Comparative protein modelling by satisfaction of spatial restraints. *J. Mol. Biol. 234*, 779−815.
(50) Brooks, B. R., Brooks, C. L., III, Mackerell, A. D., Jr., Nilsson, L., Petrella, R. J., Roux, B., Won, Y., Archontis, G., Bartels, C., Boresch, S., Caflisch, A., Caves, L., Cui, Q., Dinner, A. R., Feig, M., Fischer, S., Gao, J., Hodoscek, M., Im, W., Kuczera, K., Lazaridis, T., Ma, J., Ovchinnikov, V., Paci, E., Pastor, R. W., Post, C. B., Pu, J. Z., Schaefer, M., Tidor, B., Venable, R. M., Woodcock, H. L., Wu, X., Yang, W., York, D. M., and Karplus, M. (2009) CHARMM: The biomolecular simulation program. *J. Comput. Chem. 30*, 1545−1614.
(51) MacKerell, A. D., Jr., Bashford, D., Bellott, M., Dunbrack, R. L., Jr., Evanseck, J. D., Field, M. J., Fischer, S., Gao, J., Guo, H., Ha, S., Joseph-McCarthy, D., Kuchnir, L., Kuczera, K., Lau, F. T. K., Mattos, C., Michnick, S., Ngo, T., Nguyen, D. T., Prodhom, B., Reiher, W. E., III, Roux, B., Schlenkrich, M., Smith, J. C., Stote, R., Straub, J., Watanabe, M., Wiórkiewicz-Kuczera, J., Yin, D., and Karplus, M. (1998) All-Atom Empirical Potential for Molecular Modeling and Dynamics Studies of Proteins. *J. Phys. Chem. B 102*, 3586−3616.
(52) Mackerell, A. D., Jr., Feig, M., and Brooks, C. L., III (2004) Extending the treatment of backbone energetics in protein force fields: Limitations of gas-phase quantum mechanics in reproducing protein conformational distributions in molecular dynamics simulations. *J. Comput. Chem. 25*, 1400−1415.
(53) Bakan, A., Meireles, L. M., and Bahar, I. (2011) ProDy: Protein dynamics inferred from theory and experiments. *Bioinformatics 27*, 1575−1577.
(54) Atilgan, A. R., Durell, S. R., Jernigan, R. L., Demirel, M. C., Keskin, O., and Bahar, I. (2001) Anisotropy of fluctuation dynamics of proteins with an elastic network model. *Biophys. J. 80*, 505−515.
(55) Tobler, S. A., Sherman, N. E., and Fernandez, E. J. (2000) Tracking lysozyme unfolding during salt-induced precipitation with hydrogen exchange and mass spectrometry. *Biotechnol. Bioeng. 71*, 194−207.
(56) Wales, T. E., and Engen, J. R. (2006) Hydrogen exchange mass spectrometry for the analysis of protein dynamics. *Mass Spectrom. Rev. 25*, 158−170.
(57) Mori, H., and Ito, K. (2006) The long α-helix of SecA is important for the ATPase coupling of translocation. *J. Biol. Chem. 281*, 36249−36256.
(58) Tang, Y., Pan, X., Chen, Y., Tai, P. C., and Sui, S. F. (2011) Dimeric SecA couples the preprotein translocation in an asymmetric manner. *PLoS One 6*, e16498.
(59) Maki, J. L., Krishnan, B., and Gierasch, L. M. (2012) Using a low denaturant model to explore the conformational features of translocation-active SecA. *Biochemistry 51*, 1369−1379.
(60) Chen, H., Kim, J., and Kendall, D. A. (1996) Competition between functional signal peptides demonstrates variation in affinity for the secretion pathway. *J. Bacteriol. 178*, 6658−6664.
(61) Izard, J. W., Rusch, S. L., and Kendall, D. A. (1996) The amino-terminal charge and core region hydrophobicity interdependently contribute to the function of signal sequences. *J. Biol. Chem. 271*, 21579−21582.

(62) Kim, J., and Kendall, D. A. (1998) Identification of a sequence motif that confers SecB dependence on a SecB-independent secretory protein *in vivo*. *J. Bacteriol. 180*, 1396−1401.
(63) Miller, A., Wang, L., and Kendall, D. A. (1998) Synthetic signal peptides specifically recognize SecA and stimulate ATPase activity in the absence of preprotein. *J. Biol. Chem. 273*, 11409−11412.
(64) McMurry, J. L., and Kendall, D. A. (1999) An artificial transmembrane segment directs SecA, SecB, and electrochemical potential-dependent translocation of a long amino-terminal tail. *J. Biol. Chem. 274*, 6776−6782.
(65) Kim, J., and Kendall, D. A. (2000) Sec-dependent protein export and the involvement of the molecular chaperone SecB. *Cell Stress Chaperones 5*, 267−275.
(66) Wang, L., Miller, A., and Kendall, D. A. (2000) Signal peptide determinants of SecA binding and stimulation of ATPase activity. *J. Biol. Chem. 275*, 10154−10159.
(67) Kim, J., Miller, A., Wang, L., Muller, J. P., and Kendall, D. A. (2001) Evidence that SecB enhances the activity of SecA. *Biochemistry 40*, 3674−3680.
(68) Kebir, M. O., and Kendall, D. A. (2002) SecA specificity for different signal peptides. *Biochemistry 41*, 5573−5580.
(69) Miller, A., Wang, L., and Kendall, D. A. (2002) SecB modulates the nucleotide-bound state of SecA and stimulates ATPase activity. *Biochemistry 41*, 5325−5332.
(70) Rusch, S. L., Mascolo, C. L., Kebir, M. O., and Kendall, D. A. (2002) Juxtaposition of signal-peptide charge and core region hydrophobicity is critical for functional signal peptides. *Arch. Microbiol. 178*, 306−310.
(71) Bu, Z., Wang, L., and Kendall, D. A. (2003) Nucleotide binding induces changes in the oligomeric state and conformation of Sec A in a lipid environment: A small-angle neutron-scattering study. *J. Mol. Biol. 332*, 23−30.
(72) Wang, L., Miller, A., Rusch, S. L., and Kendall, D. A. (2004) Demonstration of a specific *Escherichia coli* SecY-signal peptide interaction. *Biochemistry 43*, 13185−13192.
(73) Rusch, S. L., and Kendall, D. A. (2007) Interactions that drive Sec-dependent bacterial protein transport. *Biochemistry 46*, 9665−9673.
(74) Rusch, S. L., and Kendall, D. A. (2007) Oligomeric states of the SecA and SecYEG core components of the bacterial Sec translocon. *Biochim. Biophys. Acta 1768*, 5−12.
(75) Sun, C., Rusch, S. L., Kim, J., and Kendall, D. A. (2007) Chloroplast SecA and *Escherichia coli* SecA have distinct lipid and signal peptide preferences. *J. Bacteriol. 189*, 1171−1175.
(76) Das, S., Stivison, E., Folta-Stogniew, E., and Oliver, D. (2008) Reexamination of the role of the amino terminus of SecA in promoting its dimerization and functional state. *J. Bacteriol. 190*, 7302−7307.
(77) Jilaveanu, L. B., Zito, C. R., and Oliver, D. (2005) Dimeric SecA is essential for protein translocation. *Proc. Natl. Acad. Sci. U.S.A. 102*, 7511−7516.
(78) Karamanou, S., Sianidis, G., Gouridis, G., Pozidis, C., Papanikolau, Y., Papanikou, E., and Economou, A. (2005) *Escherichia coli* SecA truncated at its termini is functional and dimeric. *FEBS Lett. 579*, 1267−1271.
(79) Gold, V. A., Robson, A., Clarke, A. R., and Collinson, I. (2007) Allosteric regulation of SecA: Magnesium-mediated control of conformation and activity. *J. Biol. Chem. 282*, 17424−17432.
(80) Tirion, M. M. (1996) Large Amplitude Elastic Motions in Proteins from a Single-Parameter, Atomic Analysis. *Phys. Rev. Lett. 77*, 1905−1908.
(81) Tama, F., and Sanejouand, Y. H. (2001) Conformational change of proteins arising from normal mode calculations. *Protein Eng. 14*, 1−6.
(82) Tama, F., and Brooks, C. L., III (2005) Diversity and identity of mechanical properties of icosahedral viral capsids studied with elastic network normal mode analysis. *J. Mol. Biol. 345*, 299−314.
(83) Tobi, D., and Bahar, I. (2005) Structural changes involved in protein binding correlate with intrinsic motions of proteins in the unbound state. *Proc. Natl. Acad. Sci. U.S.A. 102*, 18908−18913.
(84) Zheng, W., Brooks, B. R., and Thirumalai, D. (2006) Low-frequency normal modes that describe allosteric transitions in biological nanomachines are robust to sequence variations. *Proc. Natl. Acad. Sci. U.S.A. 103*, 7664−7669.
(85) Gouridis, G., Karamanou, S., Sardis, M. F., Scharer, M. A., Capitani, G., and Economou, A. (2013) Quaternary dynamics of the SecA motor drive translocase catalysis. *Mol. Cell 52*, 655−666.
(86) Driessen, A. J. (1993) SecA, the peripheral subunit of the *Escherichia coli* precursor protein translocase, is functional as a dimer. *Biochemistry 32*, 13190−13197.